

## Original Article

# HER2-targeted multimodal imaging of anaplastic thyroid cancer

Weijun Wei<sup>1,3</sup>, Dawei Jiang<sup>3</sup>, Zachary T Rosenkrans<sup>2</sup>, Todd E Barnhart<sup>4</sup>, Jonathan W Engle<sup>4</sup>, Quanyong Luo<sup>1</sup>, Weibo Cai<sup>2,3,4,5</sup>

<sup>1</sup>Department of Nuclear Medicine, Shanghai Jiao Tong University Affiliated Sixth People's Hospital, 600 Yishan Road, Shanghai 200233, China; <sup>2</sup>School of Pharmacy, Departments of <sup>3</sup>Radiology, <sup>4</sup>Medical Physics, University of Wisconsin-Madison, Madison, Wisconsin 53705, United States; <sup>5</sup>University of Wisconsin Carbone Cancer Center, Madison, Wisconsin 53705, United States

Received October 1, 2019; Accepted October 12, 2019; Epub November 1, 2019; Published November 15, 2019

**Abstract:** Clinical management of anaplastic thyroid cancer (ATC) is very challenging due to its dedifferentiation and aggressiveness. We aim to develop HER2-targeted multimodal imaging approaches and assess the diagnostic efficacies of these molecular imaging probes in preclinical ATC models. Flow cytometry was used to detect HER2 expression status in thyroid cancer cell lines. We then developed a HER2-specific immunoPET imaging probe <sup>89</sup>Zr-Df-pertuzumab by radiolabeling a HER-2 specific monoclonal antibody (mAb) pertuzumab with <sup>89</sup>Zr (t<sub>1/2</sub>=78.4 h) and a fluorescent imaging probe IRDye 800CW-pertuzumab. The diagnostic efficacies of the probes were assessed in subcutaneous and orthotopic ATC models, followed by ex vivo biodistribution profile and immunofluorescence staining studies. HER2 was highly expressed on the surface of all the four primary thyroid cancer cell lines examined, which included two ATC cell lines (i.e., 8505C and THJ-16T). PET imaging with <sup>89</sup>Zr-Df-pertuzumab clearly visualized all the subcutaneous ATCs with a peak tumor uptake of 20.23±6.44 %ID/g (n=3), whereas the highest tumor uptake of the nonspecific probe <sup>89</sup>Zr-Df-IgG in subcutaneous ATC models was 6.30±0.95 %ID/g (n=3). More importantly, <sup>89</sup>Zr-Df-pertuzumab PET imaging strategy readily delineated all the orthotopic ATCs with a peak tumor uptake of 24.93±8.53 %ID/g (n=3). We also suggested that Cerenkov luminescence imaging (CLI) using <sup>89</sup>Zr-Df-pertuzumab and fluorescence imaging using IRDye 800CW-pertuzumab are useful tools for image-guided removal of ATCs. We demonstrate that HER2 is a promising biomarker for ATC, and multimodal imaging using <sup>89</sup>Zr-Df-pertuzumab and IRDye 800CW-pertuzumab is useful for identifying HER2-positive ATCs.

**Keywords:** Anaplastic thyroid cancer, HER2, immunoPET, Cerenkov luminescence imaging, molecular imaging, orthotopic thyroid cancer

## Introduction

Anaplastic thyroid cancer (ATC) is a deadly disease associated with a dismal prognosis [1]. Most ATCs are thought to arise from differentiated thyroid cancers (DTCs), which are characterized by frequent oncogenic mutations or fusion oncoproteins [2-4]. Unsurprisingly, a number of genetic events are reported to be involved in the initiation and progression of ATCs [5-7]. Unlike DTCs, ATCs are virtually refractory to radioiodine therapy. Traditional treatment options for patients with ATC include surgery, chemotherapy, and external beam radiation. While efforts in the past two decades have yielded novel therapeutics, such as tyro-

sine kinase inhibitors [8, 9], and the most recent immunotherapy [10], effective management of ATCs is still a clinical challenge due to its extreme virulence and genetic complexity. Therefore, exploring molecular markers for ATCs and developing marker-specific diagnostic or theranostic approaches are of clinical significance.

The human epidermal growth factor receptor 2 (HER2) gene (*ERBB2*) is aberrantly amplified in 20% to 25% of breast cancer cases [11]. The amplification and overexpression of HER2 is a typical molecular marker of human breast cancers. Several HER2-specific therapies (e.g., trastuzumab, lapatinib, and pertuzumab) have

## HER2-targeted imaging of thyroid cancer

dramatically improved the outcomes of patients with HER2-positive breast cancers [12, 13]. Outside of breast cancers, HER2 is also overexpressed or amplified in a wide range of malignancies [14, 15], including thyroid cancers [16-19]. HER2 overexpression was found in 44% of follicular thyroid cancers and in 18% of papillary thyroid cancers [20]. HER2 is also amplified in certain ATCs [5], and CUDC-101 (an inhibitor of EGFR, HER2, and HDACs) inhibited tumor growth and metastases in metastatic ATC models [21]. These studies indicate that HER2 may emerge as a potential target for developing theranostic interventions for advanced thyroid cancers.

HER2 alterations at the levels of protein and gene are traditionally determined by immunohistochemical staining and fluorescence *in situ* hybridization, respectively [22]. However, these methods lack precision and reproducibility, and are unable to assess the HER2 variability within and among patients. In this setting, immunoPET emerges as a promising option to uncover the heterogeneous status of receptor tyrosine kinases in various kinds of cancers [23, 24]. In the case of HER2, clinical studies have demonstrated that radiolabeled monoclonal antibodies (mAbs), such as <sup>64</sup>Cu-DOTA-trastuzumab [25, 26], <sup>89</sup>Zr-Df-trastuzumab [27-29], and <sup>89</sup>Zr-Df-pertuzumab [30], are capable of evaluating HER2 heterogeneity in lesions inaccessible by traditional biopsy.

In this study, we hypothesized that HER2 is a promising target for ATC, developed a HER2 specific PET imaging probe <sup>89</sup>Zr-Df-pertuzumab, and investigated the diagnostic efficacy of the radiotracer in subcutaneous (S.C.) and orthotopic ATC models. At the same time, the burden of orthotopic ATCs was monitored by IRDye 800CW-pertuzumab fluorescence imaging. Inspired by the fact that clinical Cerenkov luminescence imaging (CLI) with <sup>131</sup>I clearly visualized superficial thyroid gland [31], we further explored CLI using <sup>89</sup>Zr-Df-pertuzumab in orthotopic ATC models.

### Methods

#### *Cell lines and flow cytometry*

The six thyroid cancer cell lines used in this study were kindly provided by Dr. Heather Hardin (University of Wisconsin-Madison), and

were maintained in RPMI 1640 medium (Gibco) supplemented with 10% FBS (Gibco) and 1% PenStrep (Invitrogen) at 37°C in a humidified atmosphere with 5% CO<sub>2</sub>. Flow cytometry was performed to evaluate the cell surface abundance of HER2 in these thyroid cancer cell lines following our previously reported protocol with minor modifications [14]. Briefly, thyroid cancer cells (1×10<sup>6</sup> cells for each sample) were suspended and washed in cold phosphate-buffered saline (PBS, HyClone). Thereafter, the cells were re-suspended in flow cytometry staining buffer (Invitrogen), incubated with 10 µg/mL of pertuzumab or Df-pertuzumab on ice for 45 min, and then washed three times with cold PBS. After re-suspending in cold flow cytometry staining buffer, cells were incubated with Alexa Fluor 488-labeled goat anti-human IgG (5 µg/mL) for 45 min and again washed with cold PBS for three times. The cell samples were re-suspended in cold PBS and analyzed using a BD LSR Fortessa flow cytometer (BD Biosciences). Flow results were analyzed with FlowJo software (FlowJo LLC).

#### *Subcutaneous and orthotopic thyroid cancer models*

All animal experiments were conducted in compliance with the institutional guidelines at the University of Wisconsin-Madison. We chose the newly established THJ-16T cell line to establish ATC models, as this cell line is known for its aggressiveness and high tumor take rate in athymic nude mice [32]. For S.C. thyroid cancer models, 5×10<sup>6</sup> THJ-16T cells were suspended in sterile PBS and mixed with matrigel matrix (Corning) at a ratio of 1:1. The prepared cells were injected subcutaneously in the right lateral flanks of athymic female nude mice aged 3-4 weeks (Envigo). For orthotopic ATC models, 0.5-1×10<sup>6</sup> THJ-16T cells were injected into the right thyroid bed as described in a previously reported protocol [33]. S.C. and orthotopic tumors were ready for imaging five weeks and four weeks after inoculation, respectively. The burden of the orthotopic ATCs was evaluated using a near-infrared imaging probe IRDye 800CW-pertuzumab, which was prepared by conjugating IRDye 800CW (LI-COR Biosciences Inc.) to pertuzumab (Roche AG) at a dye-to-mAb ratio of 1.67:1 [34]. Two weeks after tumor cell implantation, 80 µg of IRDye 800CW-pertuzumab was intravenously injected to each mouse,

## HER2-targeted imaging of thyroid cancer

and serial fluorescent imaging was obtained using an In Vivo Imaging System (IVIS, Perkin Elmer Inc.) with 745 nm/800 nm excitation/emission filters.

### *Preparation of $^{89}\text{Zr}$ -Df-pertuzumab and $^{89}\text{Zr}$ -Df-IgG*

The method for *p*-SCN-Bn-Deferoxamine (Df, Macrocyclus) conjugation and  $^{89}\text{Zr}$  radiolabeling of Df-modified mAb was previously established [35]. Briefly, 2 mg of clinical-grade pertuzumab was diluted in 400  $\mu\text{L}$  sterile PBS. The pH of the mAb solution was adjusted to 9.0 by adding 0.1 M  $\text{Na}_2\text{CO}_3$ . 5  $\mu\text{L}$  of *p*-SCN-Bn-Deferoxamine dissolved in DMSO at a concentration of 20 mg/mL was added to the mAb solution, resulting in a Df-to-mAb molar ratio of 10:1. The reaction mixture was incubated for 2 h at room temperature using a thermomixer at 600 r.p.m. The mixture was purified using a PD-10 desalting column (GE Healthcare) and Df-pertuzumab was collected.  $^{89}\text{Zr}$  was produced using a GE PETtrace biomedical cyclotron by irradiation of natural yttrium targets at the University of Wisconsin - Madison. For  $^{89}\text{Zr}$  radiolabeling, 3 mCi of  $^{89}\text{Zr}$  in oxalic acid was adjusted to a final pH of 7.0-7.5 in 0.5 M HEPES buffer (pH 7.1-7.3). 300  $\mu\text{g}$  of Df-pertuzumab was added to the above  $^{89}\text{Zr}$  solution and the mixture was left under constant shaking (600 r.p.m.) at 37°C for 1 h followed by purification of  $^{89}\text{Zr}$ -Df-pertuzumab using rinsed size exclusion PD-10 columns. Following the same procedure,  $^{89}\text{Zr}$ -labeled human serum IgG (Invitrogen) was prepared and used as a nonspecific imaging probe.

### *Small animal imaging and data analysis*

PET images were acquired using an Inveon micro-PET/CT scanner (Siemens Preclinical Solutions). Female athymic nude mice bearing THJ-16T tumors were intravenously injected with 7.4-11.1 MBq of  $^{89}\text{Zr}$ -Df-pertuzumab or  $^{89}\text{Zr}$ -Df-IgG ( $n=3$  for each group). At indicated time-points (i.e., 4 h, 24 h, 48 h, 72 h, and 96 h) post-injection (p.i.) of the radiotracers, mice were anesthetized with 2% of isoflurane mixed with oxygen and then placed in prone position on the PET scanning bed. 40 million coincidence events were collected at the initial 4 time-points, whereas 20 million coincidence events were acquired at the last time-point. PET data was reconstructed using the Inveon™

Research Workplace (Siemens Preclinical Solutions) with a non-scatter-corrected three-dimensional ordered subset expectation optimization/maximum a posteriori (OSEM3D/MAP) algorithm. Quantitative region-of-interests (ROIs) were drawn on PET images and uptake of the tracers in tumors and in major organs (i.e., blood, liver, spleen, kidney, muscle) was calculated in terms of percentage of injected dose per gram (%ID/g).

Serial CLI was performed in mice bearing orthotopic THJ-16T tumors 24 h after intravenous injection of  $^{89}\text{Zr}$ -Df-pertuzumab. The IVIS Spectrum preclinical imaging system was used to obtain the Cerenkov images. Following the manufacturer's protocol, mice were placed in the supine position in the imaging chamber and sequential 2 min acquisitions were obtained. Images were analyzed with Living Image 4.5.2 (Perkin Elmer Inc.) and expressed as photons per second per square centimeter per steradian (p/s/cm<sup>2</sup>/sr).

### *Biodistribution studies*

After PET imaging at the terminal imaging time-point (i.e., 96 h after administration of the tracers), *ex vivo* biodistribution study was carried out. First, mice were euthanized by  $\text{CO}_2$  asphyxiation. Second, blood was drawn by cardiac puncture with insulin syringes, and major organs including tumors were harvested and wet-weighed using a XSE 205 dual range analytical balance (Mettler Toledo). The radioactivity was counted with an automatic Wizard<sup>2</sup> gamma counter (Perkin Elmer). Results of the biodistribution studies were also recorded as %ID/g (mean  $\pm$  SD).

### *Histology and immunofluorescence imaging*

Tumor tissues were collected after PET imaging at the terminal time-point. The tumor tissues were either initially fixed in 10% formaldehyde for 24 h and transferred to 70% alcohol for subsequent hematoxylin and eosin (H&E) staining or embedded in optimal cutting temperature (O.C.T.) compound stored at -80°C, and used for immunofluorescent staining until most of the  $^{89}\text{Zr}$  was decayed (10 half-times, approximately 30 days). For confocal immunofluorescent staining, slides of 10  $\mu\text{m}$  were cut from O.C.T.-fixed specimens. The slides were left drying at room temperature for 15 min, fixed with

## HER2-targeted imaging of thyroid cancer

**Table 1.** Information of the six thyroid cancer cell lines used in the present study

Cell line	Year	Type	Nidus	Patient information	Mutations	Ref.
THJ-16T	2010	ATC	Primary	Female, age unspecified	<i>TP53, RB, PIK3CA<sup>E545K</sup></i>	[32]
FTC-133	1989	FTC	Primary	A 42-year-old man	<i>PTEN, TP53, TERT<sup>C228T</sup></i>	[37]
8505C	1994	ATC	Primary	A 78-year-old woman	<i>BRAF<sup>V600E</sup>, TERT<sup>C250T</sup></i>	[39]
TPC-1	1987	PTC	Primary	Female, adult	<i>TERT<sup>C228T</sup>, RET/PTC1</i>	[36]
FTC-236	1992	FTC	Metastatic	A 42-year-old man	Not available	[38]
FTC-238	1992	FTC	Metastatic	A 42-year-old man	Not available	[38]

Abbreviations: ATC, anaplastic thyroid cancer; FTC, follicular thyroid cancer; PTC, papillary thyroid cancer.

4% paraformaldehyde for 10 min, rinsed with PBS for 3 times, permeabilized with 0.2% Triton X-100 (Thermo Scientific) in PBS for 15 min, and rinsed again with PBS. Then the slides were blocked with 5% donkey serum for 1 h, followed by incubation of 15 µg/mL of pertuzumab and 20 µg/mL of rat anti-mouse CD31 antibody (Novus) overnight at 4°C. Next, the slides were washed with PBS for 3 times before a 1 h incubation with the secondary antibodies in darkness, i.e., Alexa Fluor488-labeled goat anti-human IgG (5 µg/mL, Invitrogen) and Cy3-labeled donkey anti-rat IgG (5 µg/mL, Jackson ImmunoResearch Laboratories). After washing, the slides were mounted with UltraCruz® Hardset Mounting Medium containing 1.5 µg/mL of DAPI (Santa Cruz Biotechnology), and images were obtained using a Nikon A1R confocal microscope.

### Statistical analysis

Prism software (version 7.0; GraphPad) was used for all statistical analyses. Differences between two groups were calculated using an unpaired Student's t-test. Multiple t-tests (one unpaired t-test per row) were used to compare the differences between ROI data and *ex vivo* biodistribution data from S.C. and orthotopic ATC models. One-way ANOVA was used to calculate differences in the CLI data at different time-points.  $P < 0.05$  (\*),  $P < 0.01$  (\*\*), and  $P < 0.001$  (\*\*\*) were considered statistically significant.

### Results

#### *HER2 is a potential marker for primary thyroid cancers*

We included six thyroid cancer cell lines with different origins and genetic background in our present study (Table 1) [36-39]. The expression

of HER2 on the surface of the six thyroid cancer cell lines was first assessed using flow cytometry (Figure 1). The results showed that all the four primary thyroid cancer cell lines (i.e., THJ-16T, 8505C, TPC-1, and FTC-133) were positive for HER2. However, HER2 expression was not observed in the two metastatic follicular thyroid cancer (FTC) cell lines (i.e., FTC-236 and FTC-238), where the former cell line was established from FTC cervical lymph node metastasis and the latter from FTC lung metastasis [38]. We observed a preferential level of HER2 in the two ATC cell lines tested (THJ-16T and 8505C). The high expression of HER2 on the two ATC cell lines warranted our further investigation of HER2 as a target for developing diagnostic approaches for ATCs.

#### *<sup>89</sup>Zr-Df-pertuzumab PET imaging of S.C. ATCs*

Since ATC is the most aggressive form of thyroid cancers and remains lethal in most patients, we investigated HER2 as a marker to develop molecular imaging probes for this disease. ATC models were prepared by inoculating THJ-16T cells subcutaneously into the right lateral flanks of female athymic nude mice [32]. We first explored the diagnostic efficacy of <sup>89</sup>Zr-Df-pertuzumab PET in the delineation of S.C. ATCs. In accordance with above *in vitro* results, PET imaging using <sup>89</sup>Zr-Df-pertuzumab clearly visualized all the S.C. THJ-16T tumors. Representative maximum intensity projection (MIP) and coronal PET images demonstrated substantial overexpression of HER2 in S.C. THJ-16T tumors (Figure 2), reflecting the overall and regional uptake of <sup>89</sup>Zr-Df-pertuzumab across the mouse, respectively. ROI analysis of PET images revealed an increasing tumor uptake of <sup>89</sup>Zr-Df-pertuzumab over the imaging time (Figure 2C). While the tumor uptake of <sup>89</sup>Zr-Df-pertuzumab at the initial four time-points was  $7.43 \pm 2.78$  %ID/g,  $17.87 \pm 3.74$  %ID/g,

## HER2-targeted imaging of thyroid cancer

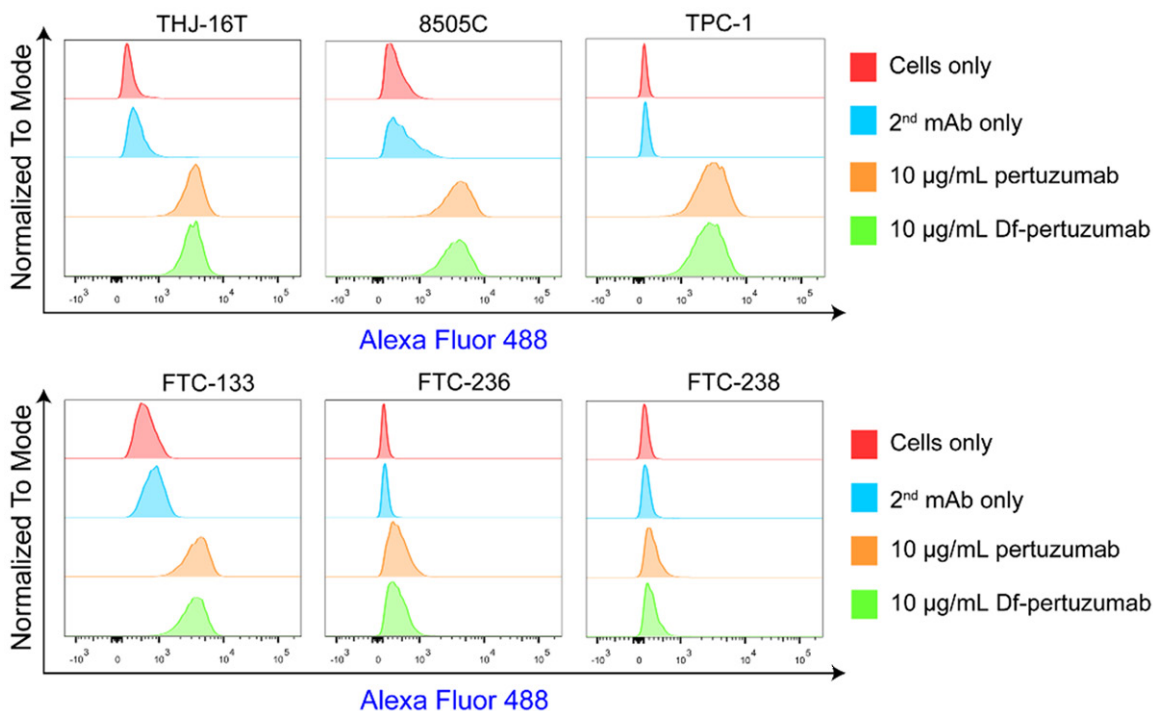


**Figure 1.** Assessment of HER2 expression in thyroid cancer cell lines by flow cytometry. Expression of HER2 is much more abundant in primary thyroid cancer cell lines (i.e., THJ-16T, 8505C, TPC-1, and FTC-133) than in metastatic thyroid cancer cell lines (i.e., FTC-236 and FTC-238).

17.57±5.77 %ID/g and 19.83±5.85 %ID/g, the peak uptake with a value of 20.23±6.44 %ID/g occurred 4 days after administration of the tracer (n=3). In contrast, uptake and retention of the tracer in blood circulation and other major organs decreased gradually over the imaging period (**Figure 2C**). The uptake in the liver, spleen, and kidney at the last imaging time-point were 8.23±1.77 %ID/g, 6.60±0.44 %ID/g, 6.13±1.65 %ID/g, respectively. These results were further corroborated by quantitative *ex vivo* biodistribution studies (**Figure 2D**). It is worthwhile to note that bone uptake (8.02±3.61 %ID/g, n=3) was caused by the unbound <sup>89</sup>Zr which preferentially accumulates in the bones. These results were further supported by confocal immunofluorescence staining and imaging of the resected tumor tissue, where abundant HER2 expression was observed on the membranes of THJ-16T cells (**Figure 2E**).

### <sup>89</sup>Zr-Df-IgG PET imaging of S.C. ATCs

As a comparison, we next examined whether <sup>89</sup>Zr-Df-IgG PET was capable of visualizing ATCs in another cohort of nude mice bearing S.C.

THJ-16T tumors. It was clear that <sup>89</sup>Zr-Df-IgG PET imaging could barely map HER2 expression and the tumors when compared with above <sup>89</sup>Zr-Df-pertuzumab PET imaging (**Figure 3**). ROI analysis showed that tumor accumulation of <sup>89</sup>Zr-Df-IgG at 4 h, 24 h, 48 h, 72 h and 96 h after injection of the tracer was 3.37±0.32 %ID/g, 5.70±0.36 %ID/g, 6.23±0.36 %IDf/g, 6.27±0.90 %ID/g, 6.30±0.95 %ID/g, respectively (n=3, **Figure 3C**). Except for the uptake at the first time-point, a direct comparison of the ROI data revealed that tumor uptake of <sup>89</sup>Zr-Df-pertuzumab was statistically higher than that of <sup>89</sup>Zr-Df-IgG at all the other time-points (P<0.05). Since the nonspecific human IgG has no antigen-specific targeting property, <sup>89</sup>Zr-Df-IgG primarily resided in the blood circulation and other major organs/tissues but not in the tumors, as shown by the *ex vivo* biodistribution studies (**Figure 3D**).

### Multimodal imaging of orthotopic ATCs

Due to their reproducibility and ability to replicate the histopathological scenario of advanced thyroid cancers, orthotopic models of human thyroid cancers hold great potential for testing

## HER2-targeted imaging of thyroid cancer

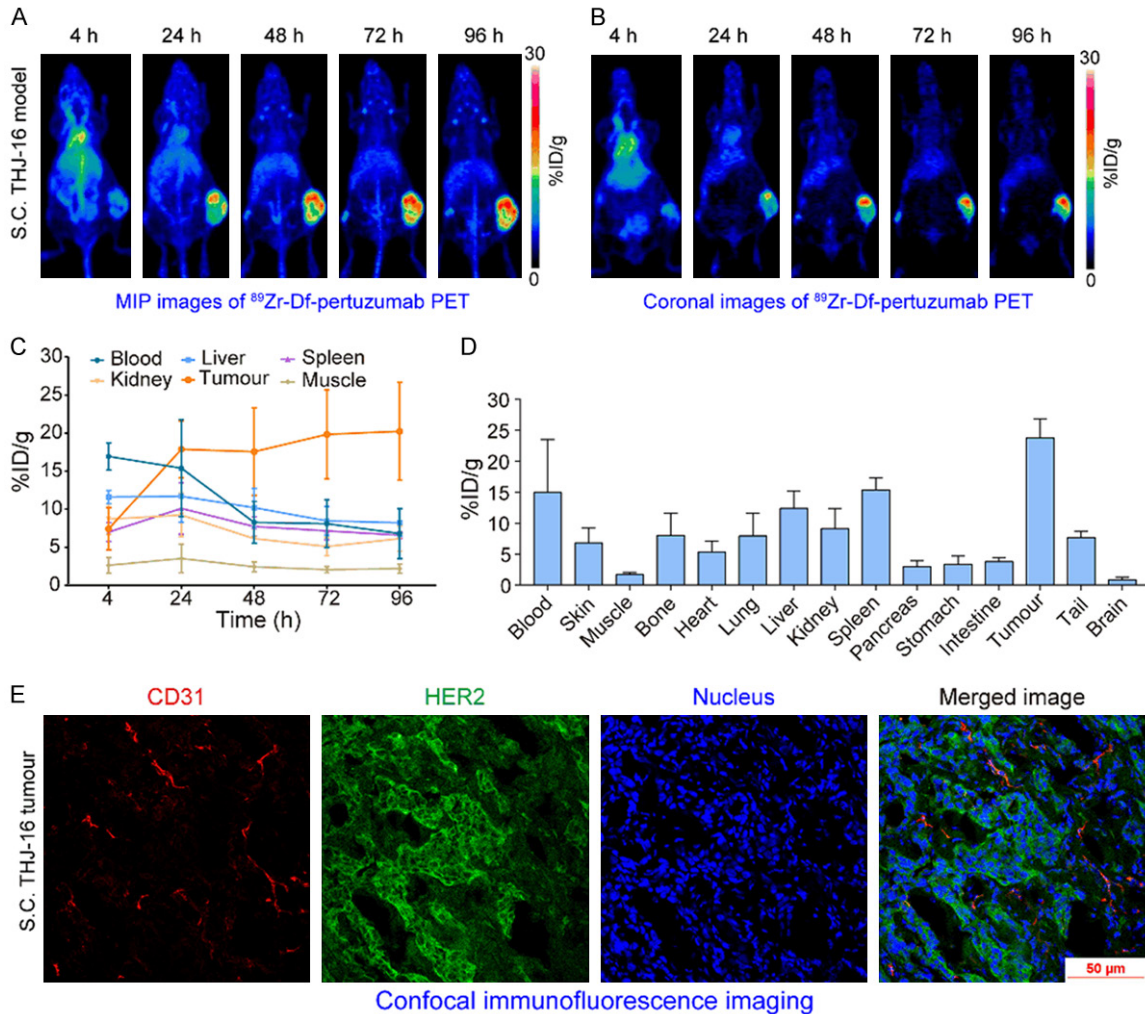


**Figure 2.** <sup>89</sup>Zr-Df-pertuzumab PET imaging of athymic nude mice bearing subcutaneous (S.C.) THJ-16T tumors. A, B. Representative maximum intensity projection (MIP) and coronal PET images showing the capability of <sup>89</sup>Zr-Df-pertuzumab PET in visualizing the tumors by imaging HER2 status. C. Quantitative analysis of change of <sup>89</sup>Zr-Df-pertuzumab in blood circulation and in other major organs over the imaging duration. D. Ex vivo biodistribution profiles in THJ-16T-bearing nude mice at 96 h after tail vein injection of <sup>89</sup>Zr-Df-pertuzumab. E. Section of S.C. THJ-16T tumor was stained with CD31 (red), HER2 (green) and DAPI (blue) and images were taken at 20× original magnification. For ROI and biodistribution data, values are shown in mean ± SD (n=3).

novel therapeutic agents and diagnostic probes. We established orthotopic ATC models using THJ-16T cell line and evaluated the tumor burden two weeks after inoculation. Serial near-infrared fluorescent imaging using IRDye 800CW-pertuzumab demonstrated signal in terms of radiant efficiency in the thyroid areas, indicating the rapid formation of orthotopic ATCs and a tumor take rate of 100% (Figure 4).

After another two weeks, we performed <sup>89</sup>Zr-Df-pertuzumab PET imaging to map HER2 expression and to detect the orthotopic THJ-16T tumors. We observed substantial uptake of

<sup>89</sup>Zr-Df-pertuzumab in the tumors as early as 24 h p.i. of the probe (Figure 5A, 5B). Quantitative analysis of ROI data illustrated that uptake of the radiotracer in the tumors increased in a time-dependent manner with the peak uptake of  $24.93 \pm 8.53$  %ID/g reached at 96 h (n=3, Figure 5C), but it was not statistically different from the corresponding uptake ( $20.23 \pm 6.44$  %ID/g, n=3) obtained in the S.C. ATC models. However, statistical analysis of the ex vivo biodistribution data showed that tumor uptake of <sup>89</sup>Zr-Df-pertuzumab was significantly higher in the orthotopic models compared to the S.C. ATC models ( $36.62 \pm 2.62$  %ID/g versus

## HER2-targeted imaging of thyroid cancer

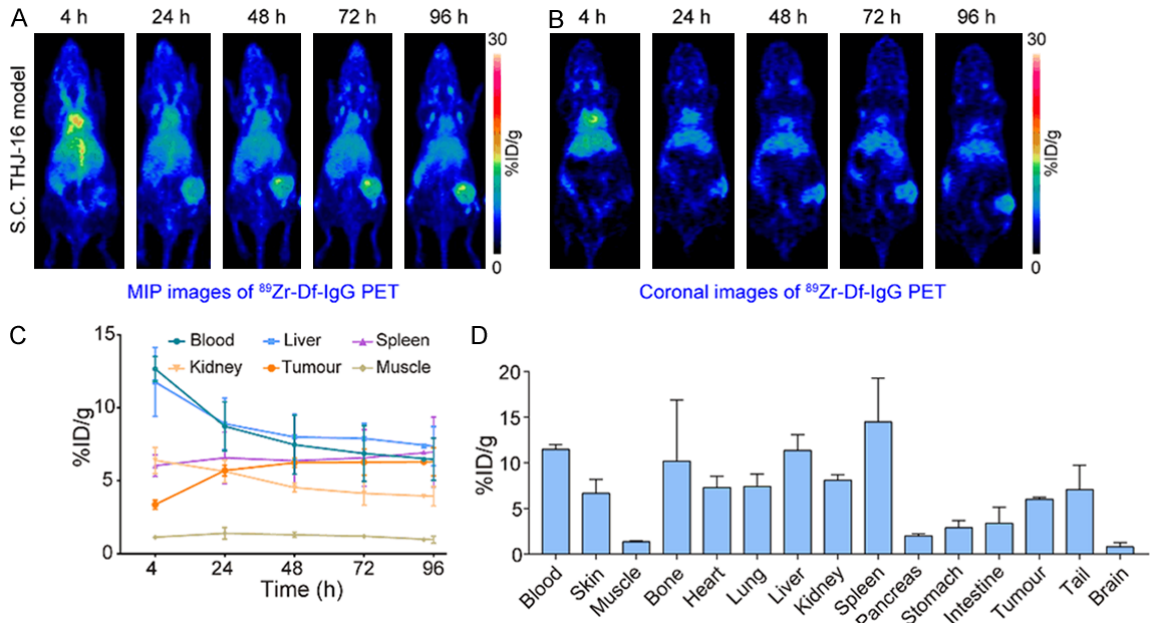
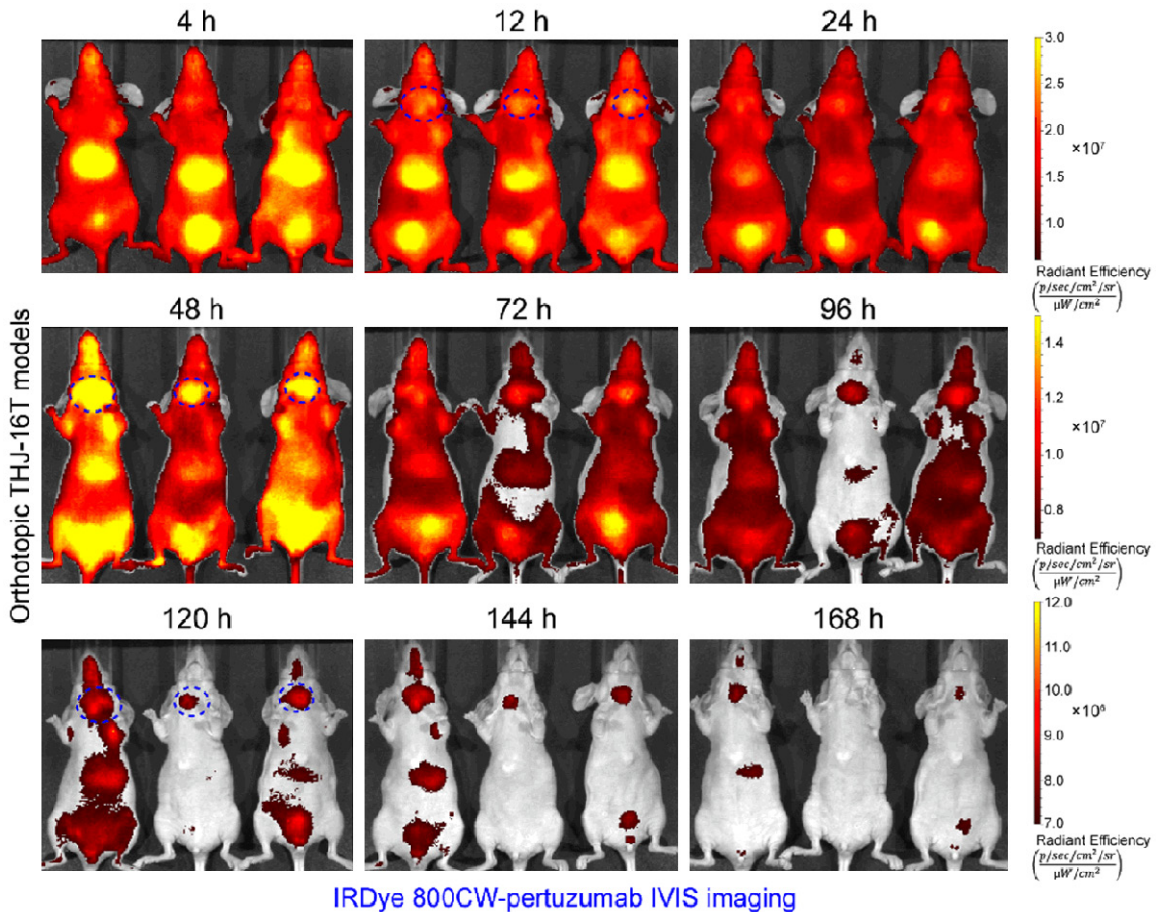


**Figure 3.**  $^{89}\text{Zr}$ -Df-IgG PET imaging of athymic nude mice bearing subcutaneous (S.C.) THJ-16T tumors. A, B. Representative maximum intensity projection (MIP) and coronal PET images performed with  $^{89}\text{Zr}$ -Df-IgG PET in nude mice bearing THJ-16T xenografts. C. Quantitative analysis of change of  $^{89}\text{Zr}$ -Df-IgG in blood circulation and major organs over the study duration. D. *Ex vivo* biodistribution profiles in THJ-16T-bearing nude mice at 96 h after tail vein injection of  $^{89}\text{Zr}$ -Df-IgG. For ROI and biodistribution data, values are shown in mean  $\pm$  SD (n=3).



## HER2-targeted imaging of thyroid cancer

**Figure 4.** Fluorescent Imaging in orthotopic anaplastic thyroid cancer (ATC) models. THJ-16T cells were inoculated into the right thyroids of athymic nude mice. Two weeks later, mice were intravenously injected with IRDye 800CW-pertuzumab and tumor burden was measured by serial IVIS fluorescent imaging in a standardized field of interest. The results implied the formation of tumors within two weeks after implantation.

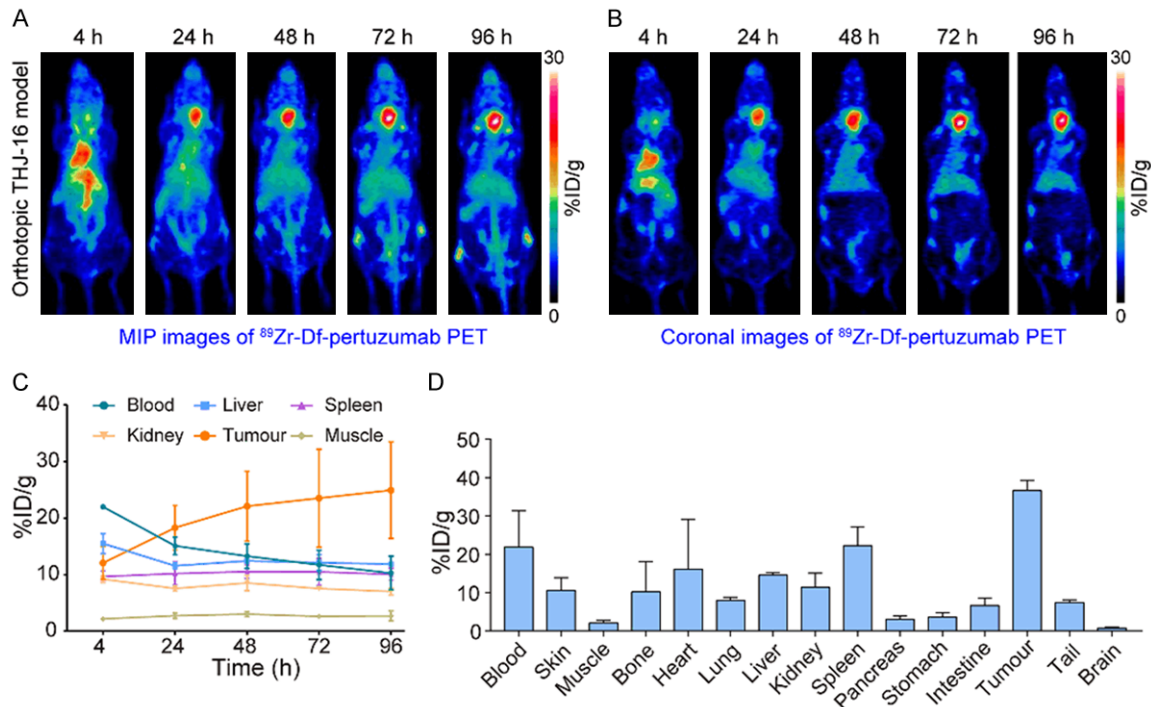


**Figure 5.** <sup>89</sup>Zr-Df-pertuzumab PET imaging clearly delineated orthotopic THJ-16T Anaplastic thyroid cancers (ATCs). Representative maximum intensity projection (MIP) images (A) and coronal images (B) showing the HER2-positive tumors. (C) ROI analysis on PET images revealed the time-dependent increase of <sup>89</sup>Zr-Df-pertuzumab uptake in the tumors and also the dynamic change of radiotracer in blood circulation and in other major organs. (D) *Ex vivo* biodistribution in THJ-16T-bearing nude mice at 96 h after tail vein injection of <sup>89</sup>Zr-Df-pertuzumab. For ROI and biodistribution data, values are shown in mean  $\pm$  SD (n=3).

23.77 $\pm$ 3.09 %ID/g,  $P < 0.01$ , n=3 for each group, **Figure 5D**).

The same orthotopic ATC models were used to evaluate the Cerenkov light-emitting efficiency of <sup>89</sup>Zr-Df-pertuzumab. CLI occurs when charged particles such as  $\alpha$ - and  $\beta$ -emitting isotopes travel faster than the velocity of light in a dielectric medium, which results in visible photon emission [40-42]. With an acquisition time of two minutes, we found that CLI clearly delineated all the orthotopic thyroid tumors (**Figure 6A**). We also found the radiance in the tumor areas reduced gradually over the imaging time. The average radiance was 19333 $\pm$ 1193 at 72 h and 15367 $\pm$ 1818 at 96 h, both of which were statistically lower than that obtained at 24 h after radiotracer administration (28933 $\pm$ 3609, n=3; **Figure 6B**). Based on these preliminary

results, we suggest that CLI using <sup>89</sup>Zr-Df-pertuzumab, upon further optimization of radiotracer dose, acquisition conditions and equipment resolution, could be harnessed to detect HER2-positive ATCs and further to facilitate image-guided surgery of the identified tumors.

### *Histology and immunofluorescence studies*

Following the orthotopic imaging studies, we euthanized the mice and collected the tumors surrounding the tracheae for histology and immunofluorescence analysis. H&E staining of the resected tumor tissue showed that pleomorphic tumor cells (large dashed inset) infiltrated thyroid gland (small inset), effacing and superseding the remaining normal thyroid follicles (**Figure 6C-E**). Consistent with the *in vivo* PET imaging results, confocal immunofluores-

## HER2-targeted imaging of thyroid cancer

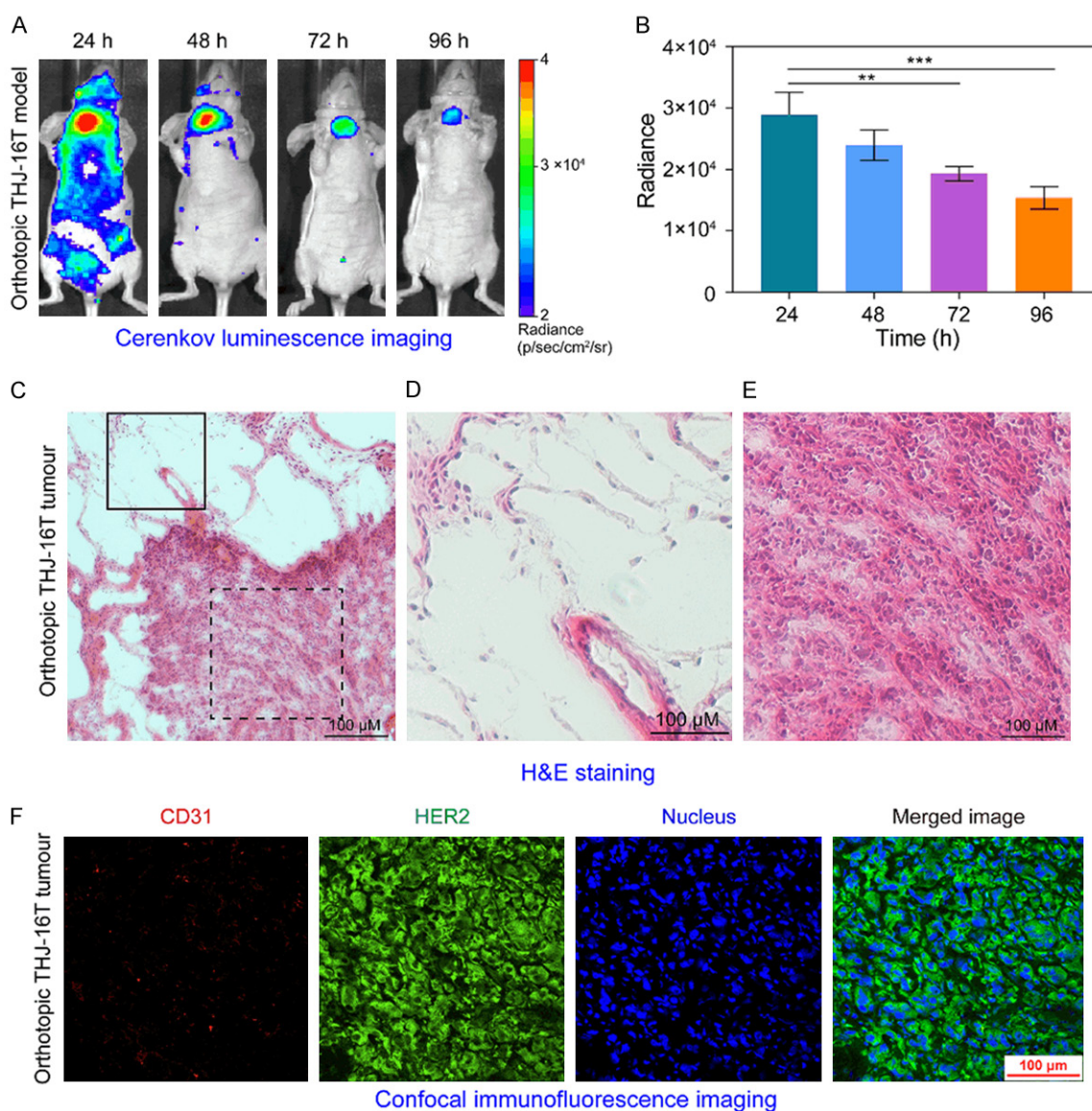


**Figure 6.** Cerenkov luminescence imaging (CLI) in orthotopic ATC models and subsequent histopathological studies. (A) CLI in the orthotopically grown xenografts using THJ-16T cells. (B) Quantitative analysis of the radiance in the thyroid areas at different time-points after administration of <sup>89</sup>Zr-Df-pertuzumab. (C-E) H&E staining of tumors showing remaining thyroid follicles (small inset, D) and THJ-16T tumor cells (large dashed inset, E). Note that the tumor cells have pleomorphic patterns, especially nuclear pleomorphism, and nuclear atypia (large dashed inset, E). (F) Section of orthotopic THJ-16T tumor was stained with CD31 (red), HER2 (green) and DAPI (blue) and images were taken at 20× original magnification. \*\*Indicates P<0.01, and \*\*\*indicates P<0.001.

cent results further confirmed the prominent expression of HER2 mainly located at the outer membranes of ATC cells (Figure 6F).

### Discussion

With an initial aim of uncovering biomarkers for advanced thyroid cancers, our results here demonstrate that HER2 is a receptor tyrosine kinase highly expressed in primary thyroid can-

cers, especially in ATCs. More importantly, our findings indicate that noninvasive molecular imaging of HER2 holds great promise for determining the HER2 status in ATCs. It has been reported that 40% of ATC cases will develop cervical lymph node metastases and 40-50% of ATC patients are suffering from distant metastases at the time of diagnosis [43]. Therefore, utilizing immuno PET in the clinic may aid comprehensive patient diagnosis and

## HER2-targeted imaging of thyroid cancer

avoid futile surgeries [44]. Furthermore, with broad clinical translation and application of  $^{89}\text{Zr}$ -Df-pertuzumab PET, this imaging approach may detect the heterogeneous levels of HER2 among the lesions throughout the whole body. That means this novel imaging tool is able to specifically identify ATC patients who might respond to HER2-targeted therapies (e.g., pertuzumab and trastuzumab), and to dynamically assess the therapeutic responses following drug administration.

It is pertinent for complete surgical resection of ATC with gross negative margins since less than 9% of ATC patients have primary tumors confined to the thyroid gland, tumors infiltrate into adjacent structures (e.g., muscle, trachea, esophagus, and larynx) in most cases [45], and negative surgical margin status is significantly predictive for improved overall survival [43]. Indocyanine green (ICG), a nonspecific fluorescent substance used for decades in various surgical procedures, preferentially distributes to tumors and/or lymph nodes through the enhanced permeability retention effect [46]. In contrast, antibodies labeled with IRDye 800CW or dual-labeled using IRDye 800CW and isotopes have high specificity for outlining tumors and for delineating tumor margins. Several ongoing clinical trials are evaluating IRDye 800CW-labeled antibodies to optimize surgical removal of malignancies [46, 47]. In a phase I protein dose escalation study, Marlène et al. reported that  $^{111}\text{In}$ -DOTA-girentuximab-IRDye 800CW, a dual-labeled probe targeting carbonic anhydrase IX, could be used intraoperatively to localize clear cell renal cell carcinomas and to delineate positive surgical margins [48]. Thus, fluorescence imaging using IRDye 800CW-pertuzumab may serve as a useful tool for image-guided complete removal of ATC upon optimization. However, in two phase I trials, which included 27 patients with head and neck squamous cell carcinomas, Gao et al. reported that toxicity from panitumumab-IRDye 800CW and cetuximab-IRDye 800CW may limit their clinical applications [49].

Alternatively, CLI using  $^{89}\text{Zr}$ -Df-pertuzumab following PET imaging may permit image-guided surgery and avoid those potential adverse effects. Indeed, optical imaging from ionizing radiation sources is a unique imaging alternative [40, 50, 51]. This is especially true for the

therapeutic isotope  $^{90}\text{Y}$ , which is very difficult to detect because of a lack of suitable  $\gamma$ -emissions and low amount of positrons emitted [52, 53]. More recently, several proof-of-concept clinical studies have demonstrated the feasibility of CLI using  $^{18}\text{F}$ -FDG [54, 55], or using  $^{131}\text{I}$  [31]. Another advantage of dual-modality imaging using  $^{89}\text{Zr}$ -Df-pertuzumab is that both PET and Cerenkov signals originate from the same probe. Upon further clinical translation,  $^{89}\text{Zr}$ -Df-pertuzumab may be integrated into the standard care of ATCs and facilitate dual-modality image-guided complete surgical resection of ATCs. Additionally, Cerenkov signals from medical isotopes can be used to trigger photodynamic therapies, as evidenced by several excellent studies [56-58], and also by our recent work [59]. Other than CLI, other potential applications of Cerenkov signal in the field of thyroid cancer needs to be exploited by future studies.

External-beam radiotherapy and chemotherapy are the mainstays for the treatment of ATCs, with the former therapy is associated with improved local disease control and overall survival [43]. Radioimmunotherapy (RIT), an alternative to traditional radiotherapy, is being developed by conjugating therapeutic radioisotopes to mAbs. RIT permits antigen-specific delivery of a high therapeutic radiation dose to cancer cells while minimizing the nonspecific radiation to normal cells [60]. RIT is gradually changing the therapeutic landscape of several kinds of malignancies including prostate cancers [61], metastatic neuroblastoma [62], and relapsed or refractory non-Hodgkin lymphoma [62, 63]. Future studies may develop HER2-targeted RIT agents by incorporating therapeutic radioisotopes (either alpha-emitting [e.g.,  $^{211}\text{At}$ ,  $^{225}\text{Ac}$ , and  $^{213}\text{Bi}$ ] or beta-emitting [e.g.,  $^{90}\text{Y}$ ,  $^{177}\text{Lu}$ , and  $^{188}\text{Re}$ ]) to antibodies (i.e., pertuzumab and trastuzumab) [60]. It is worthwhile to mention that using pretargeted strategies may further lower radiation dose to normal organs (e.g. liver), optimize the diagnostic efficacy of immunoPET probes, and enhance the therapeutic outcomes of RIT agents [64, 65]. Intensive and multimodal approaches should be used synergistically to control local and/or systemic ATC lesions. As a result, clinical outcomes of patients with ATCs will be maximized [66].

## HER2-targeted imaging of thyroid cancer

Unlike small molecule drugs that undergo rapid renal and/or hepatic clearance, mAbs are usually degraded via proteolytic catabolism after endocytosis or via internalization after forming antibody-target complex [67]. Additionally, the presence of Fc/neonatal Fc receptor interaction protects mAbs from degradation and further affects the overall biodistribution and retention of mAbs [68-70]. While  $^{89}\text{Zr}$ -Df-pertuzumab was prepared using a fully humanized IgG1 that binds to the extracellular domain II of HER2,  $^{89}\text{Zr}$ -Df-IgG was conjugated using a nonspecific human IgG. The structure differences and different targeting properties of the two mAbs may account for the different distribution profiles of the two tracers in non-targeted tissues observed in our study. Considering the fact that pertuzumab binds to the extracellular domain II of HER2 and trastuzumab selectively binds to the extracellular domain IV of HER2 [71], and addition of pertuzumab further enhances the therapeutic effect of trastuzumab and docetaxel clinically [72], future studies may investigate if it is possible to discriminate the distribution differences of trastuzumab and pertuzumab via noninvasive molecular imaging approaches. Knowledge in this regard may help clinical combinational use of pertuzumab and trastuzumab.

### Conclusions

Our findings reported indicate that  $^{89}\text{Zr}$ -Df-pertuzumab as well as IRDye 800CW-pertuzumab are useful imaging tools that can be leveraged to reveal the HER2 status in ATCs, which may further improve the molecular diagnosis and clinical management of these lethal diseases upon clinical translation and application.

### Acknowledgements

W. Wei was sponsored by the Ph.D. Innovation Fund of Shanghai Jiao Tong University School of Medicine (No. BXJ201736) and the China Scholarship Council (No. 201706230067). Q.Y. Luo was sponsored by the Shanghai Key Discipline of Medical Imaging (No. 2017-ZZ02005) and the Natural Science Foundation of China (No. 81974271). W. Cai was partially sponsored by the University of Wisconsin-Madison and the NIH (P30CA014520). The work was also partially supported the UWCCC Flow Cytometry core facility (and NIH S10

Shared Instrumentation Grant: 1S1000D018 202-01). We are grateful to Justin Jeffery for his assistance in obtaining PET data.

### Disclosure of conflict of interest

None.

**Address correspondence to:** Quanyong Luo, Department of Nuclear Medicine, Shanghai Jiao Tong University Affiliated Sixth People's Hospital, 600 Yishan Road, Shanghai 200233, China. E-mail: luoqy@sjtu.edu.cn; Weibo Cai, University of Wisconsin-Madison, Room 7137, 1111 Highland Avenue, Madison, Wisconsin 53705-2275, United States. E-mail: wcai@uwhealth.org

### References

- [1] Smallridge RC, Marlow LA and Copland JA. Anaplastic thyroid cancer: molecular pathogenesis and emerging therapies. *Endocr Relat Cancer* 2009; 16: 17-44.
- [2] Xing M. Molecular pathogenesis and mechanisms of thyroid cancer. *Nat Rev Cancer* 2013; 13: 184-199.
- [3] Cancer Genome Atlas Research Network. Integrated genomic characterization of papillary thyroid carcinoma. *Cell* 2014; 159: 676-690.
- [4] Fagin JA and Wells SA Jr. Biologic and clinical perspectives on thyroid cancer. *N Engl J Med* 2016; 375: 1054-1067.
- [5] Kunstman JW, Juhlin CC, Goh G, Brown TC, Stenman A, Healy JM, Rubinstein JC, Choi M, Kiss N, Nelson-Williams C, Mane S, Rimm DL, Prasad ML, Höög A, Zedenius J, Larsson C, Korah R, Lifton RP and Carling T. Characterization of the mutational landscape of anaplastic thyroid cancer via whole-exome sequencing. *Hum Mol Genet* 2015; 24: 2318-2329.
- [6] Landa I, Ibrahimasic T, Boucai L, Sinha R, Knauf JA, Shah RH, Dogan S, Ricarte-Filho JC, Krishnamoorthy GP, Xu B, Schultz N, Berger MF, Sander C, Taylor BS, Ghossein R, Ganly I and Fagin JA. Genomic and transcriptomic hallmarks of poorly differentiated and anaplastic thyroid cancers. *J Clin Invest* 2016; 126: 1052-1066.
- [7] Krishnamoorthy GP, Davidson NR, Leach SD, Zhao Z, Lowe SW, Lee G, Landa I, Nagarajah J, Saqcena M, Singh K, Wendel HG, Dogan S, Tamarapu PP, Blenis J, Ghossein RA, Knauf JA, Ratsch G and Fagin JA. EIF1AX and RAS mutations cooperate to drive thyroid tumorigenesis through ATF4 and c-MYC. *Cancer Discov* 2019; 9: 264-281.

## HER2-targeted imaging of thyroid cancer

- [8] Subbiah V, Kreitman RJ, Wainberg ZA, Cho JY, Schellens JHM, Soria JC, Wen PY, Zielinski C, Cabanillas ME, Urbanowitz G, Mookerjee B, Wang D, Rangwala F and Keam B. Dabrafenib and trametinib treatment in patients with locally advanced or metastatic BRAF V600-mutant anaplastic thyroid cancer. *J Clin Oncol* 2018; 36: 7-13.
- [9] Saini S, Tulla K, Maker AV, Burman KD and Prabhakar BS. Therapeutic advances in anaplastic thyroid cancer: a current perspective. *Mol Cancer* 2018; 17: 154.
- [10] Kollipara R, Schneider B, Radovich M, Babu S and Kiel PJ. Exceptional response with immunotherapy in a patient with anaplastic thyroid cancer. *Oncologist* 2017; 22: 1149-1151.
- [11] Slamon DJ, Clark GM, Wong SG, Levin WJ, Ullrich A and McGuire WL. Human breast cancer: correlation of relapse and survival with amplification of the HER-2/neu oncogene. *Science* 1987; 235: 177-182.
- [12] Pondé N, Brandão M, El-Hachem G, Werbrouck E and Piccart M. Treatment of advanced HER2-positive breast cancer: 2018 and beyond. *Cancer Treat Rev* 2018; 67: 10-20.
- [13] Pondé NF, Zardavas D and Piccart M. Progress in adjuvant systemic therapy for breast cancer. *Nat Rev Clin Oncol* 2019; 16: 27-44.
- [14] Jiang D, Im HJ, Sun H, Valdovinos HF, England CG, Ehlerding EB, Nickles RJ, Lee DS, Cho SY, Huang P and Cai W. Radiolabeled pertuzumab for imaging of human epidermal growth factor receptor 2 expression in ovarian cancer. *Eur J Nucl Med Mol Imaging* 2017; 44: 1296-1305.
- [15] Hyman DM, Piha-Paul SA, Won H, Rodon J, Saura C, Shapiro GI, Juric D, Quinn DI, Moreno V, Doger B, Mayer IA, Boni V, Calvo E, Loi S, Lockhart AC, Erinjeri JP, Scaltriti M, Ulaner GA, Patel J, Tang J, Beer H, Selcuklu SD, Hanrahan AJ, Bouvier N, Melcer M, Murali R, Schram AM, Smyth LM, Jhaveri K, Li BT, Drilon A, Harding JJ, Iyer G, Taylor BS, Berger MF, Cutler RE Jr, Xu F, Butturini A, Eli LD, Mann G, Farrell C, Lalani AS, Bryce RP, Arteaga CL, Meric-Bernstam F, Baselga J and Solit DB. HER kinase inhibition in patients with HER2- and HER3-mutant cancers. *Nature* 2018; 554: 189-194.
- [16] Bardhan P, Bui MM, Minton S, Loftus L, Carter WB, Laronga C and Ismail-Khan R. HER2-positive male breast cancer with thyroid cancer: an institutional report and review of literature. *Ann Clin Lab Sci* 2012; 42: 135-139.
- [17] Sugishita Y, Kammori M, Yamada O, Poon SS, Kobayashi M, Onoda N, Yamazaki K, Fukumori T, Yoshikawa K, Onose H, Ishii S, Yamada E and Yamada T. Amplification of the human epidermal growth factor receptor 2 gene in differentiated thyroid cancer correlates with telomere shortening. *Int J Oncol* 2013; 42: 1589-1596.
- [18] Zhu X, Zhu YJ, Kim DW, Meltzer P and Cheng SY. Activation of integrin-ERBB2 signaling in undifferentiated thyroid cancer. *Am J Cancer Res* 2014; 4: 776-788.
- [19] Handkiewicz-Junak D, Swierniak M, Rusinek D, Oczko-Wojciechowska M, Dom G, Maenhaut C, Unger K, Detours V, Bogdanova T, Thomas G, Likhitarov I, Jaksik R, Kowalska M, Chmielik E, Jarzab M, Swierniak A and Jarzab B. Gene signature of the post-chernobyl papillary thyroid cancer. *Eur J Nucl Med Mol Imaging* 2016; 43: 1267-1277.
- [20] Ruggeri RM, Campenni A, Giuffrè G, Giovannella L, Siracusa M, Simone A, Branca G, Scarfi R, Trimarchi F, Ieni A and Tuccari G. HER2 analysis in sporadic thyroid cancer of follicular cell origin. *Int J Mol Sci* 2016; 17.
- [21] Zhang L, Zhang Y, Mehta A, Boufraquech M, Davis S, Wang J, Tian Z, Yu Z, Boxer MB, Kiefer JA, Copland JA, Smallridge RC, Li Z, Shen M and Kebebew E. Dual inhibition of HDAC and EGFR signaling with CUDC-101 induces potent suppression of tumor growth and metastasis in anaplastic thyroid cancer. *Oncotarget* 2015; 6: 9073-9085.
- [22] Sauter G, Lee J, Bartlett JM, Slamon DJ and Press MF. Guidelines for human epidermal growth factor receptor 2 testing: biologic and methodologic considerations. *J Clin Oncol* 2009; 27: 1323-1333.
- [23] Cai W, Niu G and Chen X. Multimodality imaging of the HER-kinase axis in cancer. *Eur J Nucl Med Mol Imaging* 2008; 35: 186-208.
- [24] Wei W, Ni D, Ehlerding EB, Luo QY and Cai W. PET imaging of receptor tyrosine kinases in cancer. *Mol Cancer Ther* 2018; 17: 1625-1636.
- [25] Mortimer JE, Bading JR, Colcher DM, Conti PS, Frankel PH, Carroll MI, Tong S, Poku E, Miles JK, Shively JE and Raubitschek AA. Functional imaging of human epidermal growth factor receptor 2-positive metastatic breast cancer using (64)Cu-DOTA-trastuzumab PET. *J Nucl Med* 2014; 55: 23-29.
- [26] Mortimer JE, Bading JR, Park JM, Frankel PH, Carroll MI, Tran TT, Poku EK, Rockne RC, Raubitschek AA, Shively JE and Colcher DM. Tumor uptake of (64)Cu-DOTA-trastuzumab in patients with metastatic breast cancer. *J Nucl Med* 2018; 59: 38-43.
- [27] Dijkers EC, Oude Munnink TH, Kosterink JG, Brouwers AH, Jager PL, de Jong JR, van Dongen GA, Schroder CP, Lub-de Hooge MN and de Vries EG. Biodistribution of 89Zr-trastuzumab and PET imaging of HER2-positive lesions in patients with metastatic breast cancer. *Clin Pharmacol Ther* 2010; 87: 586-592.
- [28] Gebhart G, Lamberts LE, Wimana Z, Garcia C, Emonts P, Ameye L, Stroobants S, Huizing M,

## HER2-targeted imaging of thyroid cancer

- Aftimos P, Tol J, Oyen WJ, Vugts DJ, Hoekstra OS, Schroder CP, Menke-van der Houven van Oordt CW, Guiot T, Brouwers AH, Awada A, de Vries EG and Flamen P. Molecular imaging as a tool to investigate heterogeneity of advanced HER2-positive breast cancer and to predict patient outcome under trastuzumab emtansine (T-DM1): the ZEPHIR trial. *Ann Oncol* 2016; 27: 619-624.
- [29] Ulaner GA, Hyman DM, Ross DS, Corben A, Chandarlapaty S, Goldfarb S, McArthur H, Erinjeri JP, Solomon SB, Kolb H, Lyashchenko SK, Lewis JS and Carrasquillo JA. Detection of HER2-positive metastases in patients with HER2-negative primary breast cancer using <sup>89</sup>Zr-trastuzumab PET/CT. *J Nucl Med* 2016; 57: 1523-1528.
- [30] Ulaner GA, Lyashchenko SK, Riedl C, Ruan S, Zanzonico PB, Lake D, Jhaveri K, Zeglis B, Lewis JS and O'Donoghue JA. First-in-human human epidermal growth factor receptor 2-targeted imaging using (<sup>89</sup>Zr)-pertuzumab PET/CT: dosimetry and clinical application in patients with breast cancer. *J Nucl Med* 2018; 59: 900-906.
- [31] Spinelli AE, Ferdeghini M, Cavedon C, Zivelonghi E, Calandrino R, Fenzi A, Sbarbati A and Boschi F. First human cerenkography. *J Biomed Opt* 2013; 18: 20502.
- [32] Marlow LA, D'Innocenzi J, Zhang Y, Rohl SD, Cooper SJ, Sebo T, Grant C, McIver B, Kasperbauer JL, Wadsworth JT, Casler JD, Kennedy PW, Highsmith WE, Clark O, Milosevic D, Netzel B, Cradic K, Arora S, Beaudry C, Grebe SK, Silverberg ML, Azorsa DO, Smallridge RC and Copland JA. Detailed molecular fingerprinting of four new anaplastic thyroid carcinoma cell lines and their use for verification of RhoB as a molecular therapeutic target. *J Clin Endocrinol Metab* 2010; 95: 5338-5347.
- [33] Nucera C, Nehs MA, Mekeel M, Zhang X, Hodin R, Lawler J, Nose V and Parangi S. A novel orthotopic mouse model of human anaplastic thyroid carcinoma. *Thyroid* 2009; 19: 1077-1084.
- [34] Hernandez R, Sun H, England CG, Valdovinos HF, Ehlerding EB, Barnhart TE, Yang Y and Cai W. CD146-targeted immunoPET and NIRF imaging of hepatocellular carcinoma with a dual-labeled monoclonal antibody. *Theranostics* 2016; 6: 1918-1933.
- [35] Vosjan MJ, Perk LR, Visser GW, Budde M, Jurek P, Kiefer GE and van Dongen GA. Conjugation and radiolabeling of monoclonal antibodies with zirconium-89 for PET imaging using the bifunctional chelate p-isothiocyanatobenzyl-desferrioxamine. *Nat Protoc* 2010; 5: 739-743.
- [36] Tanaka J, Ogura T, Sato H and Hatano M. Establishment and biological characterization of an in vitro human cytomegalovirus latency model. *Virology* 1987; 161: 62-72.
- [37] Goretzki PE, Frilling A, Simon D and Roehrer HD. Growth regulation of normal thyroids and thyroid tumors in man. *Recent Results Cancer Res* 1990; 118: 48-63.
- [38] Demeure MJ, Damsky CH, Elfman F, Goretzki PE, Wong MG and Clark OH. Invasion by cultured human follicular thyroid cancer correlates with increased beta 1 integrins and production of proteases. *World J Surg* 1992; 16: 770-776.
- [39] Ito T, Seyama T, Hayashi Y, Hayashi T, Dohi K, Mizuno T, Iwamoto K, Tsuyama N, Nakamura N and Akiyama M. Establishment of 2 human thyroid-carcinoma cell-lines (8305c, 8505c) bearing p53 gene-mutations. *Int J Oncol* 1994; 4: 583-586.
- [40] Shaffer TM, Drain CM and Grimm J. Optical imaging of ionizing radiation from clinical sources. *J Nucl Med* 2016; 57: 1661-1666.
- [41] Pandya DN, Hantgan R, Budzevich MM, Kock ND, Morse DL, Batista I, Mintz A, Li KC and Wadas TJ. Preliminary therapy evaluation of (<sup>225</sup>Ac)-DOTA-c(RGDyK) demonstrates that cerenkov radiation derived from (<sup>225</sup>Ac) daughter decay can be detected by optical imaging for in vivo tumor visualization. *Theranostics* 2016; 6: 698-709.
- [42] Chakravarty R, Siamof CM, Dash A and Cai W. Targeted  $\alpha$ -therapy of prostate cancer using radiolabeled PSMA inhibitors: a game changer in nuclear medicine. *Am J Nucl Med Mol Imaging* 2018; 8: 247-267.
- [43] Glaser SM, Mandish SF, Gill BS, Balasubramani GK, Clump DA and Beriwal S. Anaplastic thyroid cancer: prognostic factors, patterns of care, and overall survival. *Head Neck* 2016; 38 Suppl 1: E2083-2090.
- [44] Hekman MCH, Rijpkema M, Aarntzen EH, Mulder SF, Langenhuijsen JF, Oosterwijk E, Boerman OC, Oyen WJG and Mulders PFA. Positron emission tomography/computed tomography with (<sup>89</sup>Zr)-girentuximab can aid in diagnostic dilemmas of clear cell renal cell carcinoma suspicion. *Eur Urol* 2018; 74: 257-260.
- [45] Keutgen XM, Sadowski SM and Kebebew E. Management of anaplastic thyroid cancer. *Gland Surg* 2015; 4: 44-51.
- [46] Koch M and Ntziachristos V. Advancing surgical vision with fluorescence imaging. *Annu Rev Med* 2016; 67: 153-164.
- [47] Rosenthal EL, Warram JM, de Boer E, Chung TK, Korb ML, Brandwein-Gensler M, Strong TV, Schmalbach CE, Morlandt AB, Agarwal G, Hartman YE, Carroll WR, Richman JS, Clemons LK, Nabell LM and Zinn KR. Safety and tumor specificity of cetuximab-IRDye800 for surgical

## HER2-targeted imaging of thyroid cancer

- navigation in head and neck cancer. *Clin Cancer Res* 2015; 21: 3658-3666.
- [48] Hekman MC, Rijpkema M, Muselaers CH, Oosterwijk E, Hulsbergen-Van de Kaa CA, Boerman OC, Oyen WJ, Langenhuijsen JF and Mulders PF. Tumor-targeted dual-modality imaging to improve intraoperative visualization of clear cell renal cell carcinoma: a first in man study. *Theranostics* 2018; 8: 2161-2170.
- [49] Gao RW, Teraphongphom N, de Boer E, van den Berg NS, Divi V, Kaplan MJ, Oberhelman NJ, Hong SS, Capes E, Colevas AD, Warram JM and Rosenthal EL. Safety of panitumumab-IRDye800CW and cetuximab-IRDye800CW for fluorescence-guided surgical navigation in head and neck cancers. *Theranostics* 2018; 8: 2488-2495.
- [50] Xu Y, Liu H and Cheng Z. Harnessing the power of radionuclides for optical imaging: Cerenkov luminescence imaging. *J Nucl Med* 2011; 52: 2009-2018.
- [51] Shaffer TM, Pratt EC and Grimm J. Utilizing the power of cerenkov light with nanotechnology. *Nat Nanotechnol* 2017; 12: 106-117.
- [52] Lohrmann C, Zhang H, Thorek DL, Desai P, Zanzonico PB, O'Donoghue J, Irwin CP, Reiner T, Grimm J and Weber WA. Cerenkov luminescence imaging for radiation dose calculation of a (90)Y-labeled gastrin-releasing peptide receptor antagonist. *J Nucl Med* 2015; 56: 805-811.
- [53] Ehlerding EB, Ferreira CA, Aluicio-Sarduy E, Jiang D, Lee HJ, Theuer CP, Engle JW and Cai W. (86/90)Y-based theranostics targeting angiogenesis in a murine breast cancer model. *Mol Pharm* 2018; 15: 2606-2613.
- [54] Hu H, Cao X, Kang F, Wang M, Lin Y, Liu M, Li S, Yao L, Liang J, Liang J, Nie Y, Chen X, Wang J and Wu K. Feasibility study of novel endoscopic cerenkov luminescence imaging system in detecting and quantifying gastrointestinal disease: first human results. *Eur Radiol* 2015; 25: 1814-1822.
- [55] Grootendorst MR, Cariati M, Pinder SE, Kothari A, Douek M, Kovacs T, Hamed H, Pawa A, Nimmo F, Owen J, Ramalingam V, Sethi S, Mistry S, Vyas K, Tuch DS, Britten A, Van Hemelrijck M, Cook GJ, Sibley-Allen C, Allen S and Purushotham A. Intraoperative assessment of tumor resection margins in breast-conserving surgery using (18)F-FDG cerenkov luminescence imaging: a first-in-human feasibility study. *J Nucl Med* 2017; 58: 891-898.
- [56] Kotagiri N, Sudlow GP, Akers WJ and Achilefu S. Breaking the depth dependency of phototherapy with cerenkov radiation and low-radiance-responsive nanophotosensitizers. *Nat Nanotechnol* 2015; 10: 370-379.
- [57] Pratt EC, Shaffer TM, Zhang Q, Drain CM and Grimm J. Nanoparticles as multimodal photonic transducers of ionizing radiation. *Nat Nanotechnol* 2018; 13: 418-426.
- [58] Kotagiri N, Cooper ML, Rettig M, Egbulefu C, Prior J, Cui G, Karmakar P, Zhou M, Yang X, Sudlow G, Marsala L, Chanswangphuwana C, Lu L, Habimana-Griffin L, Shokeen M, Xu X, Weilbaecher K, Tomasson M, Lanza G, DiPersio JF and Achilefu S. Radionuclides transform chemotherapeutics into phototherapeutics for precise treatment of disseminated cancer. *Nat Commun* 2018; 9: 275.
- [59] Ni D, Ferreira CA, Barnhart TE, Quach V, Yu B, Jiang D, Wei W, Liu H, Engle JW, Hu P and Cai W. Magnetic targeting of nanotheranostics enhances cerenkov radiation-induced photodynamic therapy. *J Am Chem Soc* 2018; 140: 14971-14979.
- [60] Larson SM, Carrasquillo JA, Cheung NK and Press OW. Radioimmunotherapy of human tumours. *Nat Rev Cancer* 2015; 15: 347-360.
- [61] Evans-Axelsson S, Timmermand OV, Bjartell A, Strand SE and Elgqvist J. Radioimmunotherapy for prostate cancer—current status and future possibilities. *Semin Nucl Med* 2016; 46: 165-179.
- [62] Bartholoma MD. Radioimmunotherapy of solid tumors: approaches on the verge of clinical application. *J Labelled Comp Radiopharm* 2018; 61: 715-726.
- [63] England CG, Rui L and Cai W. Lymphoma: current status of clinical and preclinical imaging with radiolabeled antibodies. *Eur J Nucl Med Mol Imaging* 2017; 44: 517-532.
- [64] van de Watering FC, Rijpkema M, Robillard M, Oyen WJ and Boerman OC. Pretargeted imaging and radioimmunotherapy of cancer using antibodies and bioorthogonal chemistry. *Front Med (Lausanne)* 2014; 1: 44.
- [65] Altai M, Membreno R, Cook B, Tolmachev V and Zeglis BM. Pretargeted imaging and therapy. *J Nucl Med* 2017; 58: 1553-1559.
- [66] Molinaro E, Romei C, Biagini A, Sabini E, Agate L, Mazzeo S, Materazzi G, Sellari-Franceschini S, Ribechini A, Torregrossa L, Basolo F, Vitti P and Elisei R. Anaplastic thyroid carcinoma: from clinicopathology to genetics and advanced therapies. *Nat Rev Endocrinol* 2017; 13: 644-660.
- [67] Hendriks JJMA, Haanen JBAG, Voest EE, Schellens JHM, Huitema ADR and Beijnen JH. Fixed dosing of monoclonal antibodies in oncology. *Oncologist* 2017; 22: 1212-1221.
- [68] Ward ES, Zhou J, Ghetie V and Ober RJ. Evidence to support the cellular mechanism involved in serum IgG homeostasis in humans. *Int Immunol* 2003; 15: 187-195.
- [69] Ober RJ, Martinez C, Vaccaro C, Zhou J and Ward ES. Visualizing the site and dynamics of IgG salvage by the MHC class I-related receptor, FcRn. *J Immunol* 2004; 172: 2021-2029.

## HER2-targeted imaging of thyroid cancer

- [70] Suzuki T, Ishii-Watabe A, Tada M, Kobayashi T, Kanayasu-Toyoda T, Kawanishi T and Yamaguchi T. Importance of neonatal FcR in regulating the serum half-life of therapeutic proteins containing the Fc domain of human IgG1: a comparative study of the affinity of monoclonal antibodies and Fc-fusion proteins to human neonatal FcR. *J Immunol* 2010; 184: 1968-1976.
- [71] Capelan M, Pugliano L, De Azambuja E, Bozovic I, Saini KS, Sotiriou C, Loi S and Piccart-Gebhart MJ. Pertuzumab: new hope for patients with HER2-positive breast cancer. *Ann Oncol* 2013; 24: 273-282.
- [72] Swain SM, Baselga J, Kim SB, Ro J, Semiglazov V, Campone M, Ciruelos E, Ferrero JM, Schneeweiss A, Heeson S, Clark E, Ross G, Benyunes MC and Cortes J; CLEOPATRA Study Group. Pertuzumab, trastuzumab, and docetaxel in HER2-positive metastatic breast cancer. *N Engl J Med* 2015; 372: 724-734.